Bioelectromagnetics 39:289–298 (2018)

Effect of Pharmacological Modulation of Actin and Myosin on Collective Cell Electrotaxis

Yashar Bashirzadeh, Jonathan Poole, Shizhi Qian, and Venkat Maruthamuthu*

Department of Mechanical & Aerospace Engineering, Old Dominion University, Norfolk, Virginia

Electrotaxis—the directional migration of cells in response to an electric field—is most evident in multicellular collectives and plays an important role in physiological contexts. While most cell types respond to applied electric fields of the order of a Volt per centimeter, our knowledge of the factors influencing this response is limited. This is especially true for collective cell electrotaxis, in which the subcellular migration response within a cell has to be coordinated with coupled neighboring cells. Here, we investigated the effect of the level of actin cytoskeleton polymerization and myosin activity on collective cell electrotaxis of Madin-Darby Canine Kidney (MDCK) cells in response to a weak electric field of physiologically relevant magnitude. We modulated the polymerization state of the actin cytoskeleton using the depolymerizing agent cytochalasin D or the polymerizing agent jasplakinolide. We also modulated the contractility of the cell using the myosin motor inhibitor blebbistatin or the phosphatase inhibitor calyculin A. While all the above pharmacological treatments altered cell speed to various extents, we found that only increasing the contractility and a high level of increase/stabilization of polymerized actin had a strong inhibitory effect specifically on the directedness of collective cell electrotaxis. On the other hand, even as the effect of the actin modulators on collective cell migration was varied, most conditions of actin and myosin pharmacological modulation—except for high level of actin polymerization/stabilization—resulted in cell speeds that were similar in the absence or presence of the electric field. Our results led us to speculate that the applied electric field may largely impact the cellular apparatus specifying the polarity of collective cell migration, rather than the functioning of the migratory apparatus. Bioelectromagnetics. 39:289–298, 2018. © 2018 Wiley Periodicals, Inc.

Keywords: galvanotaxis; collective cell migration; actin polymerization; contractility; myosin inhibition

INTRODUCTION

Electrotaxis is the directional migration of cells along (or opposite to) the direction of an electric field (EF). Many types of cells have been reported to respond to EF including corneal epithelial cells and monolayers [Zhao et al., 1997; Li et al., 2012; Gao et al., 2015], human keratinocytes, either isolated, in pairs, or in groups [Nishimura et al., 1996], and tracheal epithelial cells in isolation and in monolayers [Li et al., 2012]. The majority of the aforementioned epithelial cells migrate toward the cathode. Notably, Madin-Darby Canine Kidney (MDCK) cell sheets [Li et al., 2012] have been reported to migrate toward the cathode [Cohen et al., 2014] or anode depending on the applied electric field and MDCK sub-clone [Li et al., 2012]. Electric fields of about 1 V/cm are known to endogenously arise in vivo when, for example, epithelial sheets are wounded [Zhao et al., 1996]. Monolayers of epithelial cells also respond collectively to externally imposed electric fields of similar magnitude in vitro. Epithelial sheets show greater sensitivity in their response to EF but align more slowly than cells in isolation [Lalli and Asthagiri, 2015]. This collective response exhibits greater directionality [Li et al., 2012], but the migration rate typically slows down as cell density rises [Angelini et al., 2011]. Cell–cell interactions thus play an important role in the collective response to electrotaxis.

Conflict of interest: None.

Financial support: ODU start-up funds.

*Correspondence to: Venkat Maruthamuthu, Department of Mechanical & Aerospace Engineering, Kaufman 238e, Old Dominion University, Norfolk,VA 23529. E-mail: vmarutha@odu.edu

Received for review 7 April 2017; Accepted 14 February 2018

DOI: 10.1002/bem.22119
Published online 13 April 2018 in Wiley Online Library (wileyonlinelibrary.com).

Selective inhibition of signaling molecules has enabled the identification of key players involved in the directional electrotactic migration response of single cells and cohesive monolayers [Zhao et al., 2002; Pu et al., 2007; Meng et al., 2011; Zhang et al., 2011; Allen et al., 2013; Sun et al., 2013; Guo et al., 2015; Huang et al., 2016]. For example, it has been shown that the polarized formation of lamellipodia along the cathodal edge of some epithelial cells under DC (direct current) EF induces an electrotactic response toward the cathode [Luther et al., 1983]. Accordingly, the asymmetric activation of the MAP kinase ERK1/2 was shown to regulate the cathodal redistribution of the F-actin cytoskeleton, and its inhibition impaired the speed and directedness of single corneal epithelial cell migration toward the cathode [Zhao et al., 2002]. Similarly, the inhibition of PI3K significantly decreased both speed and directionality of brain tumor-initiating cells in isolation under EF as well as that of MDCK epithelial monolayers [Li et al., 2012; Huang et al., 2016]. In addition, inhibition of PI3K switched the directional migration of single keratocytes toward the anode of an applied EF. Many of these signaling modules that influence the electrotactic response do so by acting on the actin cytoskeleton.

Previous studies modulating specific aspects of the contractile actin cytoskeleton have yielded diverse results with respect to their effect on electrotaxis. Inhibiting actin polymerization in brain tumor-initiating single cells with latrunculin B significantly weakened cell motility but their directionality toward the anode remained biased. Jasplakinolide, a promoter of actin polymerization and stabilization of F-actin, inhibited EF-induced cathodal cluster formation of muscle cells [Zhang and Peng, 2011]. Inhibition of myosin with blebbistatin, and Rho-associated kinase with Y27632, showed little effect on single keratocyte migration toward the cathode [Sun et al., 2013]. Although myosin-II regulates cell motility [Even-Ram et al., 2007] and its inhibition with blebbistatin could affect cell migration, neither cell motility nor the directionality of brain tumor-initiating cells in isolation was affected by it under EF [Huang et al., 2016]. Cathode-directed migration of single keratocytes during electrotaxis was also not affected by blebbistatin [Allen et al., 2013]. On the other hand, blebbistatin inhibited cathode-directed migration of mouse epithelial fibroblasts in isolation [Guo et al., 2015]. It also abolished the anode-directed response of keratocyte fragments [Sun et al., 2013], although it had no effect on electrotaxis of keratocyte fragments when they were treated with cAMP or cGMP which are second messengers to extracellular factors [Zhu et al., 2016].

In this work, we wanted to specifically test the extent to which both actin organization and the level of cell contractility influenced collective cell electrotaxis in response to an EF of physiologically relevant magnitude [McCaig et al., 2009]. In particular, we wanted to determine how these modulations affected the speed and directionality of the collective electrotactic response compared to a case with no directional cue. We applied a DC electric field (DCEF) on MDCK II monolayers in vitro without or with pharmacological inhibitors that tune actin organization or contractility either higher or lower. We found that only the state of higher contractility or the state of high degree of actin polymerization showed a large loss of directionality in response to DCEF. Importantly, we found that the effect of various pharmacological inhibitions on cell speed in the presence of EF was similar to their effect on random cell migration speeds within monolayers in the absence of EF for most treatments. The latter result suggests only a minor effect of the electric field on the migration machinery itself, compared to its effect on the cell polarization apparatus.

MATERIALS AND METHODS

Cell Culture

MDCK (MDCK II, generously provided by Daniel Conway, Virginia Commonwealth University, Richmond, VA) cells were cultured with DMEM (Dulbecco's modified Eagle's medium, Corning, Corning, NY) supplemented with L-Glutamine, sodium pyruvate, 1% Penicillin/Streptomycin, and 10% Fetal Bovine Serum (FBS) (Corning) at 37 °C and under 5% CO_2. For electrotaxis experiments, the chamber in which cells were plated was prepared as follows [Song et al., 2007]: first, a Polydimethylsiloxane (PDMS) well of $10 \times 8\,mm^2$ inner area was placed in a 60-mm polystyrene petri dish (to confine the cells to the PDMS well region). Then, a $30 \times 22\,mm^2$ glass coverslip was cut in two and the two halves were glued to the petri dish parallel to each other surrounding the two sides of the PDMS well (supplementary Fig. S1). Then four 3140 silicon rubber barriers were made on opposite sides of the cover slips as shown in supplementary Figure S1a. The region of the chamber confined by the PDMS well was coated with a 0.2 mg/ml solution of Col1 in 0.1 M acetic acid at 37 °C for 15 min. After washing with PBS, the cells were plated in the PDMS well and maintained in the incubator (at 37 °C and 5% CO_2) overnight to form an approximately $10 \times 8\,mm^2$ rectangular monolayer (with minor imperfections in

the vicinity of the well) adherent to the chamber substrate. Then, the PDMS well was removed, a coverslip was glued onto the sidewall coverslips, and freshly prepared media supplemented with 10 mM HEPES was added to the chamber as in supplementary Figure S1b. For experiments involving cell treatment with pharmacological inhibitors, fresh media containing 10 mM HEPES and inhibitor at the appropriate concentration as mentioned was added to the chamber 1 h prior to the experiment.

Electrotaxis Chamber

An electrotaxis chamber similar to that introduced by Song et al. [2007] was used to apply DCEF to cells in vitro. Steinberg's solution (60 mM NaCl, 0.7 mM KCl, 0.8 mM $MgSO_4.7H_2O$, 0.3 mM $Ca(NO_3)_2.4H2O$, 1.4 mM Tris base, pH 7.4) in two petri dishes was used as the electrolyte solution. Agar salt bridges were prepared as follows: 2% wt/vol agar powder was dissolved in Steinberg's solution, heated until boiling, then cooled to approximately 60 °C and then injected into Π-shaped glass tubes prepared by heating and bending 10-cm long glass tubes with a laboratory burner. The agar subsequently gelled as it cooled. The gelled agar bridges were then inserted into the chamber in contact with the cell media at the two ends of the chamber. EF of the desired direction was achieved by microscopic alignment of the two bridges. Two silver wire electrodes were inserted into the electrolytes (as in Fig. 1a), and two connectors from the poles of a DC supply (Circuit Specialists, CSI20002S, Tempe, AZ) were connected to the electrodes to close the loop. The uncertainties associated with all of the following voltage and current

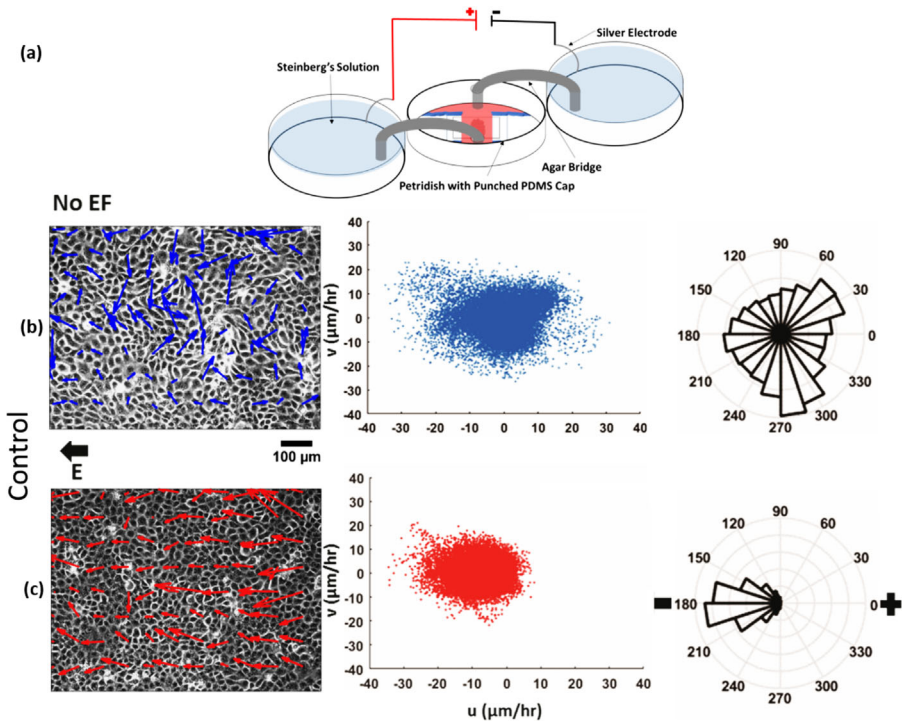

Fig. 1. Collective electrotaxis of MDCK cells in the absence of any pharmacological modulation. (**a**) Schematic illustration of sample configuration used for application of DC EF to monolayer (based on set-up in Song et al. [2007]; please see *Materials and Methods* section). (**b**) Phase image of a $860 \times 640\ \mu m^2$ region of monolayer superimposed with average local velocity vectors (averaged over 1 h) at different locations within region as determined using PIV. A scatter plot of all of the average local cell velocity components for local cell velocities and a rose plot of their angular distribution are shown on the right (based on a total of $\sim 4 \times 10^4$ velocity vectors). (**c**) Phase image of a $860 \times 640\ \mu m^2$ region of the monolayer subject to an electric field of 0.53 ± 0.03 V/cm superimposed with average local velocity vectors (averaged over 1 h) at different locations within region as determined using PIV. Electric field direction is indicated above (labelled "E" with direction). A scatter plot of all of the average local cell velocity components for local cell velocities and a rose plot of their angular distribution are shown on right (based on a total of $\sim 4 \times 10^4$ velocity vectors). Directedness was $d = 0.81$. For angular rose plots, cathode is at 180° and anode at 0°.

values are due to limited increment values of the digital read-outs (from two independent measurements). The voltage applied by the power supply was 20 ± 1 V leading to a voltage of 2.40 ± 0.12 V and a current of 0.17 ± 0.01 mA measured via a multimeter (M-1750 Elenco, Wheeling, IL) between the ends of the agar bridges in the cell chamber, with a distance of 4.5 ± 0.1 cm between them. The magnitude of the EF across the chamber was thus calculated to be 0.53 ± 0.03 V/cm.

Pharmacological Inhibitors

The pharmacological inhibitors jasplakinolide (Cayman Chemical, Ann Arbor, MI), cytochalasin D (MP Biomedicals, Santa Ana, CA), blebbistatin (Cayman Chemical), and calyculin A (MP Biomedicals, Santa Ana, CA) were used in the following concentrations: Cytochalasin D was effective at 0.2 μM as assessed by immunofluorescence (supplementary Fig. S2). Blebbistatin was used at 20 μM as its solubility was reported to decrease beyond this concentration [Várkuti et al., 2016]. Higher concentrations such as 50 μM also resulted in MDCK cell–cell contact breakage (supplementary Fig. S3). Calyculin A was used at 5 μM, the concentration at which contractility-dependent traction forces have been specifically shown to increase [Stricker et al., 2011]. Jasplakinolide is typically used in a relatively wider range (1–500 nM) of concentrations [Wan et al., 2011]. We thus used jasplakinolde at 1 nM (low), 50 nM (high), and 500 nM (highest)—use at 500 nM resulted in MDCK cell-cell contact breakage and disruption of monolayer integrity and hence was excluded from further consideration. It is important to note that pharmacological inhibitions as assessed above do not imply complete inhibition of intended biochemical targets.

Time-Lapse Imaging of Electrotaxis

The electrotaxis experiments were imaged using an inverted microscope (DMI8, Leica Microsystems, Wetzlar, Germany) equipped with an air stream incubator (Nevtek, Williamsville, VA). The petri dishes' caps were replaced with a PDMS cap with punched holes to install the agar bridges into the chamber as in Figure 1a. Electrolyte solutions were then connected with DC power supply via silver electrodes. Figure 1a shows the electrotaxis chamber equipped with electrochemical equipment for application of DCEF. From the MDCK II monolayer of area $\sim 10 \times 10\,\text{mm}^2$, phase images of the cells within multiple positions in the central region (of $\sim 5 \times 4$ mm^2 area) of the monolayer were captured by time-lapse imaging—first with no EF for at least 1 h and then upon EF application for 2 h. Two independent experiments were conducted for each case, without or with EF, or without or with specified pharmacological inhibitor. The cell density was found to be (based on cell number data in two different regions of area $0.6\,\text{mm}^2$ each, for all cases) 1472 ± 60 cells/mm^2 for the control case, 1577 ± 52 cell/mm^2 for the blebbistatin treated case, 1367 ± 67 cells/mm^2 for the jasplakinolide (low) treated case, 1468 ± 230 cells/mm^2 for the jasplakinolide (high) treated case, and 1407 ± 13 cells/mm^2 for the calyculin A treated case. Thus, cell density variations between untreated and any inhibitor-treated case was 7% or less. In general, the cells responded to EF within 1 h and so the time lapse sequence of migration for at least a 1 h time period with no EF and a 1 h time period with EF (the time period from 1 h to 2 h after EF application, for all cases) was analyzed by PIV (particle image velocimetry).

Quantification of Cell Migration Due to Electrotaxis

PIVlab (version 1.41) [Thielicke and Stamhuis, 2014], an open source MATLAB (R2015b, MathWorks, Natick, MA) program for cross-correlation, was used to process the sequence of cell phase images during random and electrotactic cell migration. First, image preprocessing, including defining a region of interest (ROI) and removing background noise, prepared the image sequences for velocimetry [Bashirzadeh et al., 2016]. PIVlab was then used to employ the Fast Fourier Transform (FFT) method with 50% overlapped interrogation windows of 64×64 pixels^2 and 32×32 pixels^2 in two passes to quantify the displacement of the cells between successive pairs of images resulting in a velocity vector field for each successive image. The MATLAB built-in function "rose" was used to depict the directionality of monolayers in an angle histogram plot. Mean of the cosine of the angle (θ) between velocity vectors of monolayers $\left(d = \frac{\Sigma\ \cos\theta}{n}\right)$ and the direction of the electric field was used as the measure of the directedness d of the migration where n is the total number of velocity vectors calculated in different regions of the monolayer. Directedness and the speed of cells in monolayers have been calculated for each case based on $3–4.5 \times 10^4$ data points. Two-way ANOVA was used to test the statistical significance of main effects (EF vs no EF as well as inhibitor vs no inhibitor) and interaction effects (in the presence of both EF and inhibitor) with P-values <0.01 considered significant. Tukey's honest significant difference criterion was used for multiple comparisons.

Immunofluorescence

MDCK II epithelial monolayers were fixed with 4% w/v paraformaldehyde (Electron Microscopy Sciences, Hatfield, PA) and permeabilized with 0.5% v/v Triton X–100 (Thermo Fisher Scientific, Waltham, MA) following standard procedures [Maruthamuthu and Gardel, 2014]. Purified mouse anti-β-catenin (BD Transduction Laboratories, BD Biosciences, San Jose, CA) at a 1:100 dilution and phalloidin (Alexa Fluor, Thermo Fisher Scientific) at a 1:200 dilution were used to stain the cells. Rhodamine-goat anti-mouse (Thermo Fisher Scientific) secondary antibody was used at a 1:200 dilution. A 20× objective lens was used for immunofluorescence imaging.

RESULTS AND DISCUSSION

Migration of MDCK Monolayers Toward the Cathode in Response to Applied DCEF

We applied a physiologically relevant [McCaig et al., 2009] weak DC field of 0.53 ± 0.03 V/cm to MDCK II monolayers (of area $\sim 10 \times 8\,\text{mm}^2$) in the electrotaxis chamber (Fig. 1a). This EF magnitude is at the lower end in the range used to elicit a response from MDCK cells previously [Li et al., 2012; Cohen et al., 2014] and is in the range of endogenous wound EF in humans and animal cells [Barker et al., 1982; Chiang et al., 1992; Zhao et al., 2006]. We found that the MDCK cells exhibited a clear cathode-directed response ($d = 0.81$, $P < 0.01$) (Fig. 1b–d) in response to this DCEF. Although various types of single cells and epithelial sheets respond to EF, epithelial cells in isolation have been reported to respond either slower or not at all to weak EFs [Li et al., 2012]. This suggests that cell–cell coupling in epithelial sheets plays a critical role in the collective response. In fact, blocking E-cadherin or depletion of extracellular Ca^{2+}has been shown to abolish electrotaxis in MDCK monolayers [Li et al., 2012]. We therefore wanted to test if impairment of the cadherin-actin link by α-catenin knock-down would affect MDCK monolayer electrotaxis. However, we found that α-catenin knock-down inhibited even random cell migration within monolayers in the absence of EF. Expectedly, migration under EF was also essentially completely inhibited (Supplementary Video S6). This result reinforced the importance of the link between cell-cell

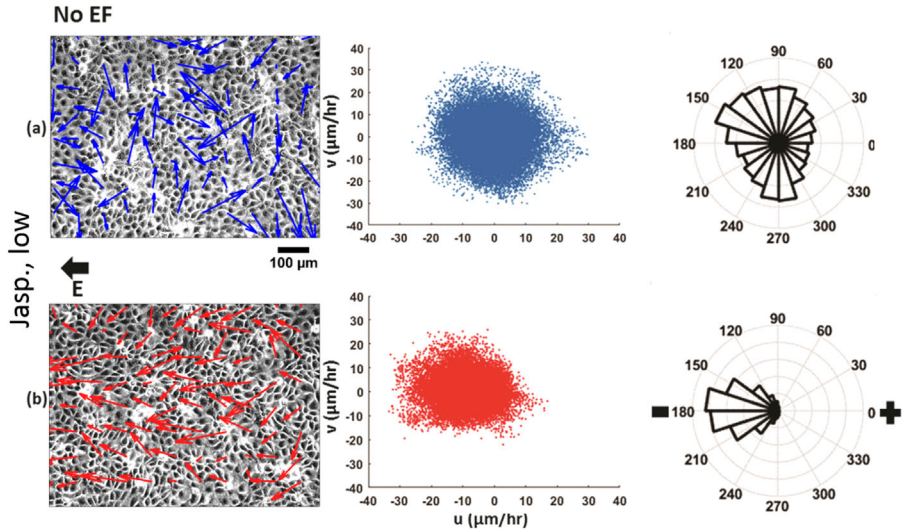

Fig. 2. (**a**) Phase image of a $860 \times 640\,\mu\text{m}^2$ region of monolayer pre-treated with 1 nM jasplakinolide superimposed with average local velocity vectors (averaged over 1 h) at different locations within region as determined using PIV. A scatter plot of all of the average local cell velocity components for local cell velocities and a rose plot of their angular distribution are shown on right (based on a total of $\sim 4.5 \times 10^4$ velocity vectors). (**b**) Phase image of a $860 \times 640\,\mu\text{m}^2$ region of monolayer pre-treated with 1 nM jasplakinolide subject to an electric field of 0.53 ± 0.03 V/cm superimposed with average local velocity vectors (averaged over 1 h) at different locations within region as determined using PIV. Electric field direction is indicated above (labelled "E" with direction). A scatter plot of all of the average local cell velocity components for local cell velocities and a rose plot of their angular distribution are shown on right (based on a total of $\sim 4.5 \times 10^4$ velocity vectors). Directedness was d = 0.74, slightly but significantly less than that for the control case ($P < 0.01$). For angular rose plots, cathode is at 180° and anode at 0°.

contacts and actin cytoskeleton of epithelial cells in cell migration within monolayers, with or without EF.

Promoting Actin Polymerization Perturbs Electrotaxis

Elongation of leading edge involving actin polymerization is one of the primary steps of cell migration and is therefore also essential during electrotaxis. To test the effect of F-actin stabilization on MDCK monolayer electrotaxis, we treated the cells with either a low (1 nM) or high (50 nM) concentration of jasplakinolide [Wan et al., 2011]. Jasplakinolide is a marine sponge toxin that induces actin polymerization [Bubb et al., 1994] and can impact the kinetic and kinematic signatures of lamellipodia [Ponti et al., 2004]. It is a potent inducer of actin polymerization in vitro by stimulation of actin filament nucleation [Bubb et al., 2000] in a manner not controlled by cellular signaling [Bubb et al., 1994; Zhang et al., 2011]. Typically, inhibiting polymer disassembly with jasplakinolide bound to actin filaments could disrupt normal cell motility [Peng et al., 2011]. Here, jasplakinolide at 1 nM treatment slightly enhanced cell migration speeds during both random cell migration with no EF and electrotactic collective response of MDCK monolayers to EF (compared to untreated case, main effect $P < 0.01$, 2-way ANOVA). Figure 2 shows a representative vector field (Fig. 2a) along with the velocity scatter plot (Fig. 2b) and directionality of the monolayer (Fig. 2c) treated with jasplakinolide. Cathode-directed electrotactic migration is slightly disturbed with 1 nM jasplakinolide treatment ($d = 0.74$, interaction effect $P < 0.01$, 2-way ANOVA). However, treatment with jasplakinolide at 50 nM led to abrogation of the cathode-directed response to EF (Fig. 3, interaction effect $P < 0.01$, 2-way ANOVA). Even though the cell velocities were largely preferentially oriented along the EF axis, as evident in the velocity scatter plot in Figure 3b, the directedness (toward the cathode) was close to zero ($d = 0.001$). On the other hand, depolymerization of actin filaments by the addition of 0.2 μM cytochalasin D [Tardieux et al., 1992] ceased collective cell migration both without and with EF (Supplementary Video S7), as expected, confirming the necessity of a basal level of F-actin to enable cell migration.

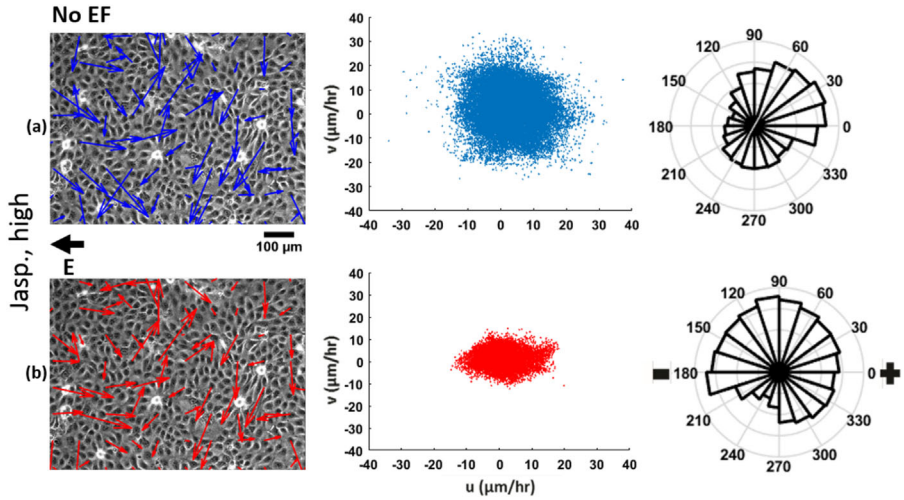

Fig. 3. (**a**) Phase image of a $860 \times 640\ \mu m^2$ region of monolayer pre-treated with 50 nM jasplakinolide superimposed with average local velocity vectors (averaged over 1 h) at different locations within region as determined using PIV. A scatter plot of all of the average local cell velocity components for local cell velocities and a rose plot of their angular distribution are shown on right (based on a total of $\sim 3 \times 10^4$ velocity vectors). (**b**) Phase image of a $860 \times 640\ \mu m^2$ region of monolayer pre-treated with 50 nM jasplakinolide subject to an electric field of 0.53 ± 0.03 V/cm superimposed with average local velocity vectors (averaged over 1 h) at different locations within region as determined using PIV. Electric field direction is indicated above (labelled "E" with direction). A scatter plot of all of the average local cell velocity components for local cell velocities and a rose plot of their angular distribution are shown on right (based on a total of $\sim 3 \times 10^4$ velocity vectors). Directedness was $d = 0.001$, significantly less than that for control case ($P < 0.01$). For angular rose plots, cathode is at 180° and anode at 0°.

Increase, but not a Decrease, in Cell Contractility Inhibits Electrotaxis

To test the role of myosin-based contractility in directional migration of cohesive monolayers, we treated the monolayer with 20 μM [Hoj et al., 2014] of blebbistatin [Straight et al., 2003]. Blebbistatin is a rapid inhibitor of myosin II ATPases [Kovács et al., 2004; Allingham et al., 2005] and thus decreases cell contractility. Here, application of blebbistatin to MDCK II monolayers slowed down both random migration of cells at no EF and their collective response to EF (compared to untreated case, main effect $P < 0.01$, 2-way ANOVA) (Fig. 4a and 4b), even though the effect of blebbistatin on the directionality of the monolayer toward the cathode under EF was not significant ($d = 0.76$, interaction effect $P = 0.57$, 2-way ANOVA) (Fig. 4c). This result suggests that reduced contractility does not impair the EF direction-sensing mechanism even though the migration speed is reduced. Slowing down of the collective cell migration of blebbistatin-treated epithelial monolayers may also reflect the disruption of the robust coupling between neighboring cells through cell-cell adhesions.

In contrast to the effect of lowering the contractility, increasing the level of contractility by treating the monolayers with 5 nM calyculin A [Kawabata and Matsuda, 2016] significantly attenuated cathode-directed electrotaxis of the MDCK monolayers ($d = 0.12$, interaction effect $P < 0.01$, 2-way ANOVA). Calyculin A inhibits protein phosphatases and thus promotes myosin activity by inhibiting myosin light chain phosphatase [Goeckeler and Wysolmerski, 1995; Stull et al., 1998]. Although cells treated with calyculin A showed impaired directedness toward the cathode under EF, calyculin A only had a minor (but statistically significant) effect on cell speed compared to the untreated case, either without or with the application of EF (compared to untreated case, main effect $P < 0.01$, 2-way ANOVA) (Fig. 5). It should be noted that while calyculin A-induced enhanced contractility has been reported in literature [Stricker et al., 2011], we cannot rule out that calyculin A-induced phosphorylation of other molecular players may have also additionally impacted the electrotactic response.

Recent experiments with keratocytes and a corresponding 'compass' model [Sun et al., 2013] suggest

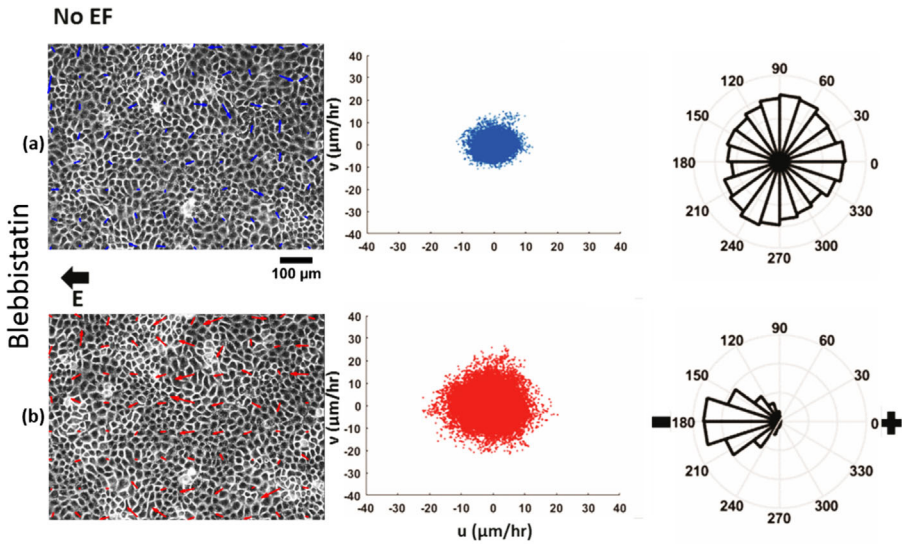

Fig. 4. (**a**) Phase image of a 860 × 640 μm^2 region of monolayer pre-treated with 20 μM blebbistatin superimposed with average local velocity vectors (averaged over 1 h) at different locations within region as determined using PIV. A scatter plot of all of the average local cell velocity components for local cell velocities and a rose plot of their angular distribution are shown on right (based on a total of ~3 × 10^4 velocity vectors). (**b**) Phase image of a 860 × 640 μm^2 region of the monolayer pre-treated with 20 μM blebbistatin subject to an electric field of 0.53 ± 0.03 V/cm superimposed with average local velocity vectors (averaged over 1 h) at different locations within region as determined using PIV. Electric field direction is indicated above (labelled "E" with direction). A scatter plot of all of the average local cell velocity components for local cell velocities and a rose plot of their angular distribution are shown on right (based on a total of ~3 × 10^4 velocity vectors). Directedness was $d = 0.76$, slightly but significantly less than that for control case ($P < 0.01$). For angular rose plots, cathode is at 180° and anode at 0°.

that two competing intracellular pathways bias a cell along the direction of the applied EF. Actin polymerization influences the strength of the "frontness" cue [Sun et al., 2013] in this model, directing the cells toward the cathode whereas contractility promotes migration toward the anode by inducing the rear of the cell to point toward the cathode. The effect of calyculin A on collective cell electrotaxis as reported here is consistent with the proposed compass model [Sun et al., 2013] of electrotaxis: higher contractility as a result of treatment with calyculin A may promote the "backness" cue to point toward the cathode (and the cell to point toward the anode) in opposition to the cells' normal electrotactic response toward the cathode. These opposing factors could well have resulted in the low level of directedness as reported above upon calyculin A treatment. In contrast, decrease of contractility using blebbistatin is expected to suppress the backness cue, leaving the frontness cue to dominate and point toward the cathode as in the untreated case. Promoting actin polymerization with a low concentration of jasplakinolide is expected to similarly maintain cathode directedness by promoting the frontness cue, but higher jasplakinolide concentrations may impair the dynamic rearrangements of the actin cytoskeleton that are still necessary for persistent migration.

Electric Field Appears to Largely Affect Cell Polarity Rather than Cell Migration Speeds

Electrotactic cell motility was affected to various extents by the specific pharmacological agents used in this study. The differential effect of these treatments on cell speed in the presence of EF was statistically significant in all cases. However, we wanted to assess the magnitude of change affected by these different inhibitor treatments in the absence or presence of EF. Figure 6 compares the average random speeds in the absence of EF and electrotactic migration speeds in the presence of EF of inhibitor-treated monolayers. Except for jasplakinolide treatment at the higher concentration, which may have affected the cell's ability to undergo persistent directional migration, the magnitude of cell speeds without EF and with EF were similar in magnitude (although the differences among them were statistically significant, Fig. 6). These results may suggest that the EF primarily

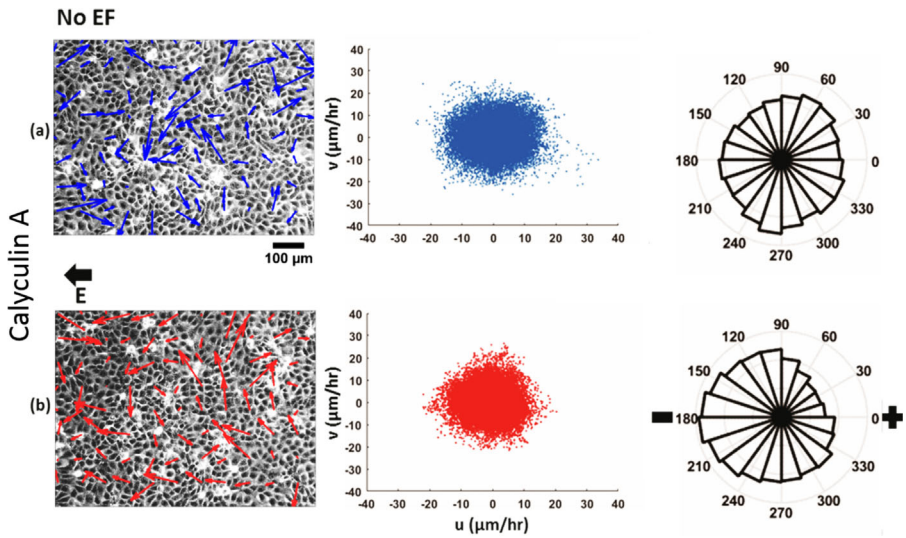

Fig. 5. (**a**) Phase image of a $860 \times 640\ \mu m^2$ region of monolayer pre-treated with 5 nM calyculin A superimposed with average local velocity vectors (averaged over 1 h) at different locations within region as determined using PIV. A scatter plot of all of the average local cell velocity components for local cell velocities and a rose plot of their angular distribution are shown on right (based on a total of $\sim 4.5 \times 10^4$ velocity vectors). (**b**) Phase image of a $860 \times 640\ \mu m^2$ region of monolayer pre-treated with 5 nM calyculin A subject to an electric field of 0.53 ± 0.03 V/cm superimposed with average local velocity vectors (averaged over 1 h) at different locations within region as determined using PIV. Electric field direction is indicated above (labelled "E" with direction). A scatter plot of all of the average local cell velocity components for local cell velocities and a rose plot of their angular distribution are shown on right (based on a total of $\sim 4.5 \times 10^4$ velocity vectors). Directedness was $d = 0.12$, significantly less than that for control case ($P < 0.01$). For the angular rose plots, cathode is at 180° and anode at 0°.

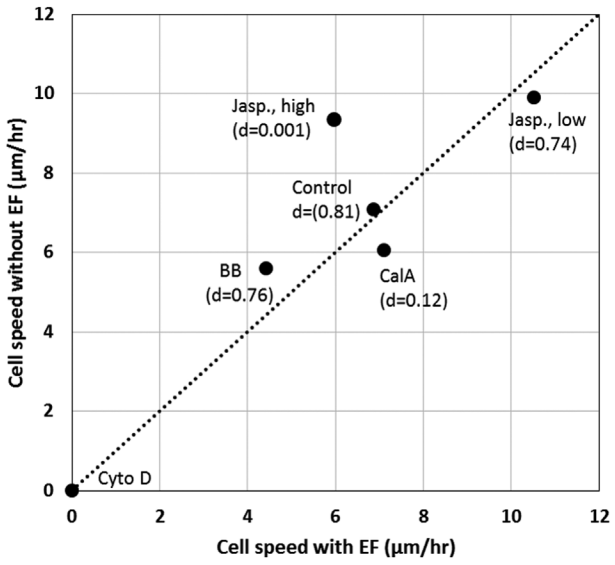

Fig. 6. Average local cell speed (filled circles) within MDCK monolayers without EF is plotted against that with EF, with control as well as different pharmacological treatments as indicated. Dotted line indicates a line of slope 1 through origin. Standard error of mean in all cases was less than the size of filled circles and therefore not depicted. Directedness of collective cell migration in each case is shown in brackets, with a directedness of 1 corresponding to uniformly directed collective migration toward cathode and a directedness of 0 corresponding to no preferential migration toward cathode.

affects the components of the cell polarization pathway rather than that of the cell migration machinery.

CONCLUSION

Cathode-directed collective migration response of MDCK monolayers to EF was tested under a range of pharmacological perturbations to the actomyosin machinery. We found that both treatment with calyculin A and the higher concentration of jasplakinolide nearly eliminated the directedness of cells in response to EF. In contrast to directedness, cell speed in the presence of EF was affected by the pharmacological agents perturbing both actin polymerization state and myosin activity to various extents. However, the motility of the cells in the monolayer in most cases was largely conserved in magnitude between the cases without and with EF, except for actin stabilization using higher jasplakinolide concentration. Based on our results, we speculate that EF has a stronger effect on cell migration directionality rather than on cell migration capacity per se during collective cell response to EF.

AUTHORS' CONTRIBUTIONS

Yashar Bashirzadeh conducted the experiments, analyzed the data, and wrote the manuscript. Jonathan Poole also conducted experiments. Shizhi Qian contributed to the design of the experiments. Venkat Maruthamuthu conceived and designed the experiments, and revised the manuscript.

REFERENCES

Allen GM, Mogilner A, Theriot JA. 2013. Electrophoresis of cellular membrane components creates the directional cue guiding keratocyte galvanotaxis. Curr Biol 23:560–568.

Allingham JS, Smith R, Rayment I. 2005. The structural basis of blebbistatin inhibition and specificity for myosin II. Nat Struct Mol Biol 12:378–379.

Angelini TE, Hannezo E, Trepat X, Marquez M, Fredberg JJ, Weitz DA. 2011. Glass-like dynamics of collective cell migration. Proc Natl Acad Sci 108:4714–4719.

Barker A, Jaffe L, Vanable J. 1982. The glabrous epidermis of cavies contains a powerful battery. Am J Physiol Regul Integr Comp Physiol 242:R358–R366.

Bashirzadeh Y, Maruthamuthu V, Qian S. 2016. Electrokinetic phenomena in pencil lead-Based microfluidics. Micromachines 7:235.

Bubb MR, Senderowicz A, Sausville EA, Duncan K, Korn ED. 1994. Jasplakinolide, a cytotoxic natural product, induces actin polymerization and competitively inhibits the binding of phalloidin to F-actin. J Biol Chem 269:14869–14871.

Bubb MR, Spector I, Beyer BB, Fosen KM. 2000. Effects of jasplakinolide on the kinetics of actin polymerization: an explanation for certain in vivo observations. J Biol Chem 275:5163–5170.

Chiang M, Robinson KR, Vanable JW. 1992. Electrical fields in the vicinity of epithelial wounds in the isolated bovine eye. Exp Eye Res 54:999–1003.

Cohen DJ, Nelson WJ, Maharbiz MM. 2014. Galvanotactic control of collective cell migration in epithelial monolayers. Nature Mater 13:409–417.

Even-Ram S, Doyle AD, Conti MA, Matsumoto K, Adelstein RS, Yamada KM. 2007. Myosin IIA regulates cell motility and actomyosin-microtubule crosstalk. Nat Cell Biol 9:299–309.

Gao J, Raghunathan VK, Reid B, Wei D, Diaz RC, Russell P, Murphy CJ, Zhao M. 2015. Biomimetic stochastic topography and electric fields synergistically enhance directional migration of corneal epithelial cells in a MMP-3-dependent manner. Acta Biomater 12:102–112.

Goeckeler ZM, Wysolmerski RB. 1995. Myosin light chain kinase-regulated endothelial cell contraction: the relationship between isometric tension, actin polymerization, and myosin phosphorylation. J Cell Biol 130:613–627.

Guo L, Xu C, Li D, Zheng X, Tang J, Bu J, Sun H, Yang Z, Sun W, Yu X. 2015. Calcium ion flow permeates cells through SOCs to promote cathode-directed galvanotaxis. PLoS ONE 10:e0139865.

Hoj JP, Davis JA, Fullmer KE, Morrell DJ, Saguibo NE, Schuler JT, Tuttle KJ, Hansen MD. 2014. Cellular contractility changes are sufficient to drive epithelial scattering. Exp Cell Res 326:187–200.

Huang YJ, Hoffmann G, Wheeler B, Schiapparelli P, Quinones-Hinojosa A, Searson P. 2016. Cellular microenvironment

modulates the galvanotaxis of brain tumor initiating cells. Sci Rep 6:21583.
Kawabata N, Matsuda M. 2016. Cell density-dependent increase in tyrosine-monophosphorylated ERK2 in MDCK cells expressing active Ras or Raf. PLoS ONE 11:e0167940.
Kovács M, Tóth J, Hetényi C, Málnási-Csizmadia A, Sellers JR. 2004. Mechanism of blebbistatin inhibition of myosin II. J Biol Chem 279:35557–35563.
Lalli ML, Asthagiri AR. 2015. Collective migration exhibits greater sensitivity but slower dynamics of alignment to applied electric fields. Cell Mol Bioeng 8:247–257.
Li L, Hartley R, Reiss B, Sun Y, Pu J, Wu D, Lin F, Hoang T, Yamada S, Jiang J. 2012. E-cadherin plays an essential role in collective directional migration of large epithelial sheets. Cell Mol Life Sci 69:2779–2789.
Luther PW, Peng HB, Lin JJ. 1983. Changes in cell shape and actin distribution induced by constant electric fields. Nature 303:61–64.
Maruthamuthu V, Gardel ML. 2014. Protrusive activity guides changes in cell-cell tension during epithelial cell scattering. Biophys J 107:555–563.
McCaig CD, Song B, Rajnicek AM. 2009. Electrical dimensions in cell science. J Cell Sci 122:4267–4276.
Meng X, Arocena M, Penninger J, Gage FH, Zhao M, Song B. 2011. PI3K mediated electrotaxis of embryonic and adult neural progenitor cells in the presence of growth factors. Exp Neurol 227:210–217.
Nishimura KY, Isseroff RR, Nuccitelli R. 1996. Human keratinocytes migrate to the negative pole in direct current electric fields comparable to those measured in mammalian wounds. J Cell Sci 109:199–207.
Peng GE, Wilson SR, Weiner OD. 2011. A pharmacological cocktail for arresting actin dynamics in living cells. Mol Biol Cell 22:3986–3994.
Ponti A, Machacek M, Gupton SL, Waterman-Storer C, Danuser G. 2004. Two distinct actin networks drive the protrusion of migrating cells. Science 305:1782–1786.
Pu J, McCaig CD, Cao L, Zhao Z, Segall JE, Zhao M. 2007. EGF receptor signalling is essential for electric-field-directed migration of breast cancer cells. J Cell Sci 120:3395–3403.
Song B, Gu Y, Pu J, Reid B, Zhao Z, Zhao M. 2007. Application of direct current electric fields to cells and tissues in vitro and modulation of wound electric field in vivo. Nat Protoc 2:1479–1489.
Straight AF, Cheung A, Limouze J, Chen I, Westwood NJ, Sellers JR, Mitchison TJ. 2003. Dissecting temporal and spatial control of cytokinesis with a myosin II Inhibitor. Science 299:1743–1747.
Stricker J, Aratyn-Schaus Y, Oakes PW, Gardel ML. 2011. Spatiotemporal constraints on the force-dependent growth of focal adhesions. Biophys J 100:2883–2893.
Stull J, Lin P, Krueger J, Trewhella J, Zhi G. 1998. Myosin light chain kinase: functional domains and structural motifs. Acta Physiol Scand 164:471–482.
Sun Y, Do H, Gao J, Zhao R, Zhao M, Mogilner A. 2013. Keratocyte fragments and cells utilize competing pathways to move in opposite directions in an electric field. Curr Biol 23:569–574.
Tardieux I, Webster P, Ravesloot J, Boron W, Lunn JA, Heuser JE, Andrews NW. 1992. Lysosome recruitment and fusion are early events required for trypanosome invasion of mammalian cells. Cell 71:1117–1130.
Thielicke W, Stamhuis E. 2014. PIVlab-towards user-friendly, affordable and accurate digital particle image velocimetry in MATLAB. J Open Res Software 2:e30.
Várkuti BH, Képiró M, Horváth IÁ, Végner L, Ráti S, Zsigmond Á, Hegyi G, Lenkei Z, Varga M, Málnási-Csizmadia A. 2016. A highly soluble, non-phototoxic, non-fluorescent blebbistatin derivative. Sci Rep 6:26141.
Wan LQ, Ronaldson K, Park M, Taylor G, Zhang Y, Gimble JM, Vunjak-Novakovic G. 2011. Micropatterned mammalian cells exhibit phenotype-specific left-right asymmetry. Proc Natl Acad Sci 108:12295–12300.
Zhang HL, Peng HB. 2011. Mechanism of acetylcholine receptor cluster formation induced by DC electric field. PLoS ONE 6:e26805.
Zhang J, Calafiore M, Zeng Q, Zhang X, Huang Y, Li RA, Deng W, Zhao M. 2011. Electrically guiding migration of human induced pluripotent stem cells. Stem Cell Rev Rep 7:987–996.
Zhao M, Agius-Fernandez A, Forrester JV, McCaig CD. 1996. Directed migration of corneal epithelial sheets in physiological electric fields. Invest Ophthalmol Vis Sci 37:2548–2558.
Zhao M, McCaig CD, Agius-Fernandez A, Forrester JV, Araki-Sasaki K. 1997. Human corneal epithelial cells reorient and migrate cathodally in a small applied electric field. Curr Eye Res 16:973–984.
Zhao M, Pu J, Forrester JV, McCaig CD. 2002. Membrane lipids, EGF receptors, and intracellular signals colocalize and are polarized in epithelial cells moving directionally in a physiological electric field. FASEB J 16:857–859.
Zhao M, Song B, Pu J, Wada T, Reid B, Tai G, Wang F, Guo A, Walczysko P, Gu Y. 2006. Electrical signals control wound healing through phosphatidylinositol-3-OH kinase-[gamma] and PTEN. Nature 442:457.
Zhu K, Sun Y, Miu A, Yen M, Liu B, Zeng Q, Mogilner A, Zhao M. 2016. CAMP and cGMP play an essential role in galvanotaxis of cell fragments. J Cell Physiol 231: 1291–1300.

SUPPORTING INFORMATION

Additional Supporting Information may be found in the online version of this article.